INSTANTON EFFECTS IN EUCLIDEAN VACUUM, REAL TIME PRODUCTION, AND IN THE LIGHT-FRONT WAVE FUNCTIONS*

Edward Shuryak, Ismail Zahed

Center for Nuclear Theory, Stony Brook University
Stony Brook, NY 11794, USA

Received 29 March 2022, accepted 31 March 2022, published online 26 April 2022

Nontrivial topological structures of non-Abelian gauge fields were discovered in the 1970s. Instanton solutions, describing vacuum tunneling through topological barriers, have fermionic zero modes which are at the origin of 't Hooft effective Lagrangian. In the 1980s, instanton ensembles have been used to explain chiral symmetry breaking. In the 1990s, a large set of numerical simulations were performed deriving Euclidean correlation functions. The special role of scalar diquarks in nucleons and color superconductivity in dense quark matter has been elucidated. In these lectures, we discuss further developments of physics related to gauge topology. We show that the instanton–anti-instanton "streamline" configurations describe "sphaleron transitions" in high-energy collisions, which result in production of hadronic clusters with nontrivial topological/chiral charges. (They are not yet observed, but discussions of dedicated experiments at the LHC and RHIC are ongoing.) Another new direction is instanton effects in hadronic spectroscopy, both in the rest frame and on the light front. We will discuss their role in central and spin-dependent potentials, form factors and anti-quark nuclear "sea". Finally, we summarize the advances in the semiclassical theory of deconfinement, and chiral phase transitions at finite temperature, in QCD, and in some of its "deformed" versions.

DOI:10.5506/APhysPolB.53.4-A1

1. Brief overview of gauge topology

We start these lectures with a map, outlining the role and interdependence of various topological structures in the QCD vacuum. The phenomenon of *color confinement* (the left blue region in Fig. 1) was first related to *center vortices*, associated with a phase π for a quark looping around, changing the sign of the linking Wilson line. Two such vortices combined

together, lead to a singularity with a phase 2π, shown by the white arrow, known as the *Dirac string*. Their ends are identified as *magnetic monopoles* (blue disks). Confinement is their *Bose–Einstein condensation*, perhaps the most physical signature of this phenomenon.

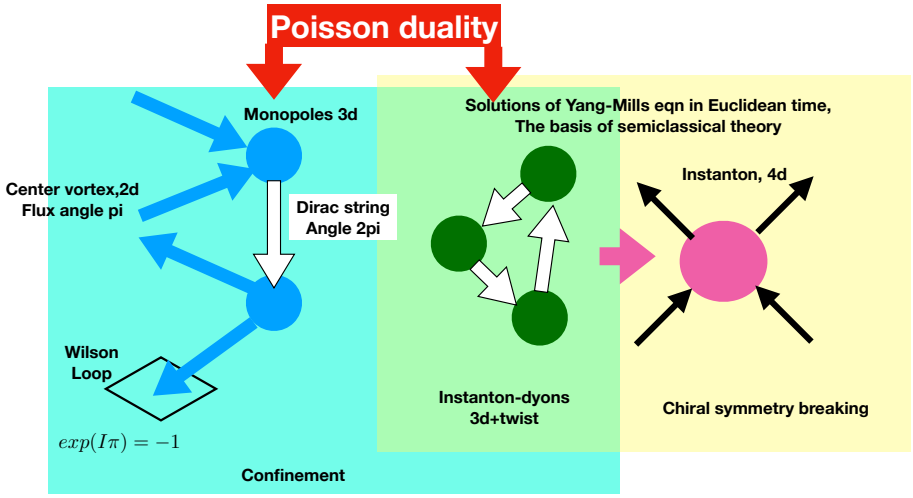

Fig. 1. Map of gauge topology, explanations are in the text.

The right yellow region of Fig. 1 is associated with another major non-perturbative phenomenon, *chiral symmetry breaking*. The pink disk refers to *instantons*, 4D solitons in Euclidean space-time. Fermions in this field have *zero modes*, elevating each instanton into the 't Hooft multi-fermion operator. The four black arrows correspond to the case of two quark flavors, u, d. The resulting 4-fermion vertex is similar to the Nambu–Jona-Lasinio hypothetical interaction, and also breaks spontaneously $\mathrm{SU}(N_\mathrm{f})_\mathrm{A}$ chiral symmetry provided the instanton density is sufficiently large.

At finite temperature, the *Polyakov line* has a number of eigenvalues or *holonomies* $\mu_i(T)$ (see below). The instanton solution amended by such asymptotics for the A_0 field splits into instanton constituents, known as *instanton-dyons* or *instanton-monopoles*[1]. Like instantons, they have topological charges. Unlike instantons, the charges are *not quantized to integers* Q. This is possible since they are connected by Dirac strings due to their magnetic charges. Ensembles of these topological objects will be shown to generate both confinement, and chiral breaking at the end of these lectures.

[1] Both names were criticized: they are neither the dyons of Schwinger, nor monopoles of Dirac, but Euclidean self-dual objects, with equal E and B up to a sign. Perhaps a new name, emphasizing their Euclidean nature, is needed: can it *e.g.* be *instantino*?

Last but not least is the phenomenon of *Poisson duality*, started as a technical observation relating partition functions derived in terms of monopoles and in terms of instanton-dyons. As we will discuss below, it has a wider meaning: their equality brings to mind equivalence of two other great approaches to classical dynamics, by Hamilton and Lagrange, respectively.

The detailed discussion of these configurations, in addition to discussions about the QCD flux tubes and holographic QCD *etc.*, can be found in [1].

2. Brief history of instantons

2.1. Semiclassical theory based on path integrals: instantons and fluctons

The quantum mechanics courses include semiclassical methods based on certain representation of the wave function, starting with the celebrated Bohr–Sommerfeld quantization condition applied to the oscillator and hydrogen atom, and followed by the Wentzel–Kramers–Brillouin (WKB) approximation, developed in 1926. Unfortunately, subsequent study has shown that generalization of those to physical systems with more than one degree of freedom, as well as to systematic order-by-order account for quantum fluctuations, is not possible.

By definition, the Feynman path integral gives the *density matrix* in coordinate representation (see *e.g.* a very pedagogical Feynman–Hibbs book)

$$\rho\left(x_{\rm i}, x_{\rm f}, t_{\rm tot}\right) = \int\limits_{x(0)=x_{\rm i}}^{x(t_{\rm tot})=x_{\rm f}} Dx(t)\, {\rm e}^{i\,S[x(t)]/\hbar}\,. \tag{1}$$

Note that it is a function of the initial and final coordinates, as well as the time needed for the transition. Here, S is the classical action of the system, *e.g.* for a particle of mass m in a static potential $V(x)$, it is

$$S = \int\limits_0^{t_{\rm tot}} {\rm d}t\, \left[\frac{m}{2}\left(\frac{{\rm d}x}{{\rm d}t}\right)^2 - V(x)\right]\,.$$

Feynman has shown that the oscillating exponent along the path provides the correct weight of the path integral (1). For reference, the same object can also be written in a form closer to that used in quantum mechanics courses. Heisenberg wrote it as a matrix element of the time evolution operator, the exponential of the Hamiltonian[2]

$$\rho\left(x_{\rm i}, x_{\rm f}, t_{\rm tot}\right) = \langle x_{\rm f}|\, {\rm e}^{i\hat{H}t_{\rm tot}}|x_{\rm i}\rangle \tag{2}$$

between states in which a particle is localized in–out.

[2] Here, we assume that the motion happens in a time-independent potential, for otherwise, the exponential is time ordered.

The Schrödinger set of stationary states $\hat{H}|n\rangle = E_n|n\rangle$ can also be used as a basis set. Since the Hamiltonian is diagonal in this basis, there is a single (not double) sum

$$\rho\left(x_{\rm i}, x_{\rm f}, t\right) = \sum_n \psi_n^*\left(x_{\rm f}\right) \psi_n(x_{\rm i})\, {\rm e}^{iE_n t} \tag{3}$$

with $\psi_n(x) = \langle n|x\rangle$. Oscillating weights for different states are often hard to calculate and one may wonder if it is possible to analytically continue in time to the Euclidean version with i absorbed into it. For reasons which will soon become clear, we will also define this imaginary time on a circle with circumference β

$$\tau = i\, t \in [0, \beta]\,.$$

In this way, we will be able to describe the *quantum+statistical* mechanics of a particle in a heat bath with temperature T related to the circle circumference

$$\beta = \frac{\hbar}{T}\,.$$

Such periodic time is known as the Matsubara time. Expression (3) is now

$$\rho(x, x, t) = \sum_n |\psi_n(x)|^2\, {\rm e}^{-E_n/T} \tag{4}$$

which sums the quantum-mechanical probabilities to find a particle at point x times its thermal weight. Performing the integral over all x and using the normalization of the weight functions, one finds the expression for the thermal partition function

$$Z = \sum_n {\rm e}^{-E_n/T}\,. \tag{5}$$

We will use this expression below in a Feynman path integral form, with *(i)* taken over all *periodic* paths with the same endpoints, and with *(ii)* Euclidean or rotated time. The probability to find a particle at a certain point is then

$$P(x_0, t_{\rm tot}) = \int\limits_{x(0)=x_0}^{x(\beta)=x_0} Dx(\tau)\, {\rm e}^{-S_{\rm E}[x(\tau)]/\hbar}\,. \tag{6}$$

Note that here, the exponent is not oscillating and equals the Euclidean action

$$S_{\rm E} = \int\limits_0^\beta {\rm d}\tau \left[\frac{m}{2}\left(\frac{{\rm d}x}{{\rm d}\tau}\right)^2 + V(x)\right] \tag{7}$$

in which the sign of the potential is reversed and the time derivative is understood to be over τ.

Looking for the periodic paths with the minimal action, one may start with the simplest, *i.e.* a particle at rest with $x(\tau) = \text{const}$! Such a path is dominant for small time (Matsubara circle), with $\beta \to 0$ (or high temperature T)[3]. If one ignores the time dependence and velocity on the paths, there is no kinetic term and only the potential one in the action contributes. Thus,

$$P(x_0, \beta) \sim \mathrm{e}^{-\frac{V(x_0)}{T}}\,, \tag{8}$$

which corresponds to the classical[4] thermal distribution for a particle in a potential V.

Since the weight is $\exp(-S[x(\tau)])$, the paths with the smallest action should give the largest contribution. These paths satisfy the classical (Euclidean) equation of motion, as we will carry below. The semiclassical approximation — the *dominance* of these paths — would be justified as soon as the corresponding action is large

$$S_{\rm cl} \equiv S[x_{\rm cl}(\tau)] \gg \hbar\,. \tag{9}$$

Such classical paths were called *fluctons* in [2]. These paths should have Euclidean time period $\beta = \hbar/T$. For simplicity, let us start with "cold" QM or vanishingly small T, $\beta \to \infty$. Little thinking of how to arrange a classical path with a very long period leads to the following solution: the particle should roll to the top of the (flipped) potential with exactly such energy as to sit there for very long time before it will roll back to the (arbitrary) point x_0 from which the path started. The classical paths corresponding to relaxation toward the potential bottom take the form of a path *climbing up* from an arbitrary point x_0 to the maximum, see Fig. 2.

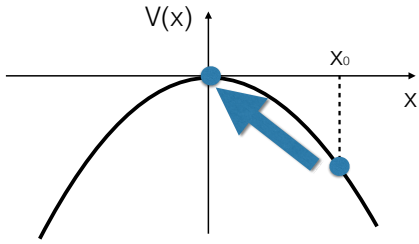

Fig. 2. Sketch of the flucton path climbing toward the (flipped) minimum of the potential.

[3] Note that it is opposite to the limit discussed above in the Hamiltonian approach.

[4] Note that if we would keep $\hbar \neq 1$, the one in β and in the exponent $\exp(-S/\hbar)$ would cancel out, confirming the classical nature of this limit.

Let us start with the harmonic oscillator as the unavoidable first example. For simplicity, let us use the canonical units, in which the particle mass is $m = 1$ and the oscillator frequency is $\Omega = 1$, so that our (Euclidean) Lagrangian[5] is simplified to

$$L_{\rm E} = \frac{\dot{x}(\tau)^2}{2} + \frac{x(\tau)^2}{2}\,. \tag{10}$$

Due to this sign, in Euclidean time τ, the oscillator does not oscillate e^{it} but relaxes $e^{-\tau}$. For a harmonic oscillator, the classical equations of motion (EOM) are of course not difficult to solve. However, it is always easier to get solutions using energy conservation (the first integral of motion for static potentials). Since we are interested in solutions with zero energy $E = 0$, they correspond to $\dot{x}^2 = 2V(x)$. The boundary conditions are x_0 at $\tau = 0$ plus periodicity on a circle with circumference β. This solution is

$$x_{\rm flucton}(\tau) = x_0\ \frac{\left(e^{\beta-\tau}\ +\ e^{\tau}\right)}{e^{\beta}+1} \tag{11}$$

defined for $\tau \in [0, \beta]$. The particle moves toward $x = 0$ and reaches some minimal value, at $\tau = \beta/2$, and then returns to the initial point x_0 again at $\tau = \beta$. Due to the periodicity in τ, one may shift its range to $\tau \in [-\beta/2, \beta/2]$. The minimal value at $\tau = \beta/2$

$$x_{\rm min} = \frac{x_0}{\cosh\left(\frac{\beta}{2}\right)} \to_{\beta\to\infty} 0$$

is exponentially small at low temperature. The climbing to the potential top at $x = 0$ is nearly accomplished, if the period is large.

The solution in the zero temperature or $\beta \to \infty$ limit simplifies to $x_0\, e^{-|\tau|}$. In the opposite limit of small β or high T, there is no time to move far from x_0, so in this case, the particle does not move at all. The classical action of the flucton path is

$$S_{\rm flucton} = x_0^2\ \tanh\left(\frac{\beta}{2}\right)\,. \tag{12}$$

The result means that the particle distribution

$$P(x_0) \sim \exp\left(-\frac{x_0^2}{\coth\left(\frac{\beta}{2}\right)}\right) \tag{13}$$

[5] Note again the flipped sign of the potential term. In Minkowski time, the potential has sign minus.

is Gaussian at any temperature. Note that the width of the distribution

$$\left\langle x^2 \right\rangle = \frac{1}{2} \coth\left(\frac{\beta}{2}\right) = \frac{1}{2} + \frac{1}{\mathrm{e}^{\beta} - 1} \tag{14}$$

is the ground-state energy plus the contribution due to the thermal excitations, which we already mentioned at the beginning of the chapter. Thus, the flucton reproduces the well-known results for the harmonic oscillator, see *e.g. Feynman's Statistical Mechanics*.

Flucton solutions for several well-used QM problems (anharmonic oscillator, quartic double well, sin-like potential) were discussed in detail in [12]. Unlike WKB, one can define and calculate semiclassical series in $\hbar$ by the well-defined procedure, using Feynman diagrams. Finite-temperature fluctons were used for anharmonic oscillator and 4-nucleon clustering in [11].

Quantum mechanical instantons were introduced[6] by [4] in the context of tunneling in the double-well potential. In the inverted potential, it is a path going from one maximum to another.

For an early pedagogical review, including the one-loop (determinant) calculation by the same tedious scattering-phase method see *ABC of instantons* [5]. Two-loop corrections were first calculated in [6], some technical errors in it were corrected by Shuryak and Wohler in [7]. Three-loop corrections have been calculated by Escobar-Ruiz, Turbiner, and Shuryak in [8].

The calculation goes in the same standard way, the path is written as a classical plus *quantum fluctuation* $\delta x(\tau)$, and then the action is expanded in powers of $\delta x(\tau)$. One technical (but important) difference between the *instantons* and *fluctons* is that in the former case the *fluctuation operator* ($O(\delta x(\tau)^2)$) has a *zero mode*, related to time-shift symmetry. Therefore, the Green function for the fluctuations needs to be defined in a *nonzero mode subspace* of the Hilbert space. This complication leads to new features, such as additional diagrams not following directly from the Lagrangian.

The Gauge theory instanton was found in the famous work by Belavin, Polyakov, Schwartz, and Tyupkin, and since known as the BPST instanton [9]. Let us recall how it was obtained, as some of the expressions will be useful for later use. To find the classical solution corresponding to tunneling, BPST used the following 4-dimensional spherical ansatz depending on the *radial* trial function f

$$gA^a_\mu = \eta_{a\mu\nu}\partial_\nu F(y)\,, \qquad F(y) = 2\int\limits_0^{\xi(y)} \mathrm{d}\xi' f\left(\xi'\right) \tag{15}$$

[6] It is interesting that the first application to the QFT problem — pairs production in constant electric field — was done already in 1931 by Sauter [3].

with $\xi = \ln(x^2/\rho^2)$ and η the 't Hooft symbol defined by

$$\eta_{a\mu\nu} = \begin{cases} \epsilon_{a\mu\nu} & \mu,\, \nu = 1,\, 2,\, 3\,, \\ \delta_{a\mu} & \nu = 4\,, \\ -\delta_{a\nu} & \mu = 4\,. \end{cases} \tag{16}$$

We also define $\bar{\eta}_{a\mu\nu}$ by changing the sign of the last two equations. Upon substitution of the gauge fields in the gauge Lagrangian $(G_{\mu\nu})^2$, one finds that the effective Lagrangian has the form of

$$L_{\text{eff}} = \int \mathrm{d}\xi \left[\frac{\dot{f}^2}{2} + 2f^2(1-f)^2 \right] \tag{17}$$

corresponding to the motion of a particle in a double-well potential. The Euclidean solution is that of a quantum mechanical instanton, connecting the *maxima* of the flipped potential. The corresponding field is

$$A^a_\mu(x) = \frac{2}{g} \frac{\eta_{a\mu\nu} x_\nu}{x^2 + \rho^2}\,. \tag{18}$$

Here, ρ is an arbitrary parameter characterizing the size of the instanton. Like in the potential we discussed in the preceding section, its appearance is dictated by the scale invariance of the classical Yang–Mills equation. The ansatz itself perhaps needs some explanation. The 't Hooft symbol projects to sefl-dual fields, which is best captured by the identity

$$S = \frac{1}{4g^2} \int \mathrm{d}^4x\, G^a_{\mu\nu} G^a_{\mu\nu} = \frac{1}{4g^2} \int \mathrm{d}^4x \left[\pm G^a_{\mu\nu} \tilde{G}^a_{\mu\nu} + \frac{1}{2} \left(G^a_{\mu\nu} \mp \tilde{G}^a_{\mu\nu} \right)^2 \right], \tag{19}$$

where $\tilde{G}_{\mu\nu} = 1/2\epsilon_{\mu\nu\rho\sigma} G_{\rho\sigma}$ is the dual field strength tensor (the field tensor in which the roles of electric and magnetic fields are interchanged). Since the first term is a topological invariant (see below) and the last term is always positive, it is clear that the action is minimal if the field is (anti)*self-dual*[7]

$$G^a_{\mu\nu} = \pm \tilde{G}^a_{\mu\nu}\,. \tag{20}$$

In a simpler language, it means that the Euclidean electric and magnetic fields are the same[8]. The action density is given by

$$\left(G^a_{\mu\nu}\right)^2 = \frac{192\rho^4}{(x^2+\rho^2)^4}\,. \tag{21}$$

[7] This condition is written in Euclidean space. In Minkowski space, there is an extra i in the electric field.

[8] In the BPST paper, the self-duality condition (1^{st} order differential equation) was solved, rather than (2^{nd} order) EOM for the quartic oscillator.

It is spherically symmetric and very well localized, at large distances, it is $\sim x^{-8}$. The action depends on the scale only via the running coupling

$$S = \frac{8\pi^2}{g^2(\rho)}\,. \tag{22}$$

The one-loop (determinant) quantum corrections were calculated in the classic paper by 't Hooft [10]. The two-loop and higher-order quantum corrections have not been calculated to this day due to the difficulties with the part of the Green functions related to the nonzero modes.

2.2. Chiral symmetry breaking in QCD

Chiral symmetries are additional symmetries that appear when quarks are massless. Since the mass term is the only one in the QCD Lagrangian connecting spinors with right (R) and left (L) chiralities, the $\mathrm{SU}(N_\mathrm{f})$ symmetry of flavor quark rotations gets doubled by acting on the L- and R-quarks separately. Also, it can be viewed as *vector* and *axial-vector* transformations, in which rotations on the L- and R-spinors are in the same or opposite directions. The latters are further split into $\mathrm{U}(1)_\mathrm{A}$ (acting on all quarks by $\exp(i\gamma_5\theta)$ and $\mathrm{SU}(N_\mathrm{f})_\mathrm{A}$.

The physics of the nonperturbative vacuum of strong interaction started even before QCD. Nambu and Jona-Lasinio (NJL) [13], inspired by BCS theory of superconductivity, have qualitatively explained that strong enough attraction of quarks can break $\mathrm{SU}(N_\mathrm{f})_\mathrm{A}$ chiral symmetry spontaneously and, among many other effects, create near-massless pions.

Instantons, the basis for a semiclassical theory of the QCD vacuum and hadrons, have been discovered in 1970s [9], and soon 't Hooft has found their fermionic zero modes and formulated his famous effective Lagrangian [10]. Not only did it solve the famous "$\mathrm{U}(1)_\mathrm{A}$ problem" — by making the η' non-Goldstone and heavy — but it also produces a strong attraction in the σ and π channels. In the framework of the so-called instanton liquid model (ILM) [14], it provided a microscopic (QCD-based) basis for chiral symmetry breaking, chiral perturbation theory, and the pion properties. Its two parameters

$$\rho = \frac{1}{3}\ \mathrm{fm}\,, \qquad n_{I+\bar{I}} = \frac{1}{R^4} = 1\ \mathrm{fm}^{-4} \tag{23}$$

play the same role as the cutoff and coupling in the NJL model. These parameters have withstood the scrutiny of time, and describe rather well the chiral dynamics related to pions, the Euclidean correlation functions in the few femtometers range, the interacting ensemble of instantons, and much more, see [15] for a review.

The subject of these lectures is many other uses of instantons discussed in recent works. We will consider quark pair production and its role in the isospin asymmetry of the nucleon "sea", the inclusion of $\bar{I}I$ molecules in mesonic form factors, and forces between quarks in hadrons.

2.3. Euclidean correlation functions

This analysis originally started from the small-distance OPE and the QCD sum rule method, it moved to intermediate distances (see review *e.g.* in [16]).

First, the experimentally known correlation functions were reproduced by the instanton liquid model at *small distances* at a quantitative level. Then, for many mesonic channels [18, 19], significant numerical efforts were made allowing to calculate the relevant correlation functions till larger distances (of about 1.5 fm), where they decay by a few decades. As a result, the predictive power of the model has been explored in substantial depth. Many of the coupling constants and even hadronic masses were calculated, with good agreement with experiment and lattice.

2.4. Diquarks and color superconductivity

Subsequent calculations of baryonic correlators [20] have revealed further surprising facts. In the instanton vacuum, the nucleon was shown to be made of a "constituent quark" plus a deeply bound *diquark*, with a mass nearly the same as that of constituent quarks. On the other hand, decuplet baryons (like Δ^{++}) had shown no such diquarks, remaining a weakly bound set of three constituent quarks. Deeply bound scalar diquarks are a direct consequence of the 't Hooft Lagrangian, a mechanism that is also shared by the Nambu–Jona-Lasinio interaction [21] but ignored for a long time.

It also leads to the realization that diquarks can become the Cooper pairs in dense quark matter, see [22] for a review on "color superconductivity".

3. The topological landscape and sphaleron production processes

There has been significant development in the understanding of the "topological landscape" in relation between instantons and sphaleron production processes, see [23]. Recently there has been a renewed interest, due to the possible experimental searches for sphaleron production at the RHIC/LHC [24]. The sphalerons are 3-dimensional, static, and purely magnetic configurations that minimize the energy functional. To quantify them, we will focus on two main variables. Their topological Chern–Simons number and their squared field size are

$$N_{\rm CS} \equiv \frac{\epsilon^{\alpha\beta\gamma}}{16\pi^2}\int {\rm d}^3x\left(A^a_\alpha\partial_\beta A^a_\gamma + \frac{1}{3}\epsilon^{abc}A^a_\alpha A^b_\beta A^c_\gamma\right), \qquad \rho^2 \equiv \frac{\int {\rm d}^3x\vec{x}^{\,2}\vec{B}^{\,2}}{\int {\rm d}^3x\vec{B}^{\,2}}. \tag{24}$$

If those are kept constant, by adding pertinent Lagrange multipliers to the action, we can find the minimal possible energy and Chern–Simons number in parametric form

$$U_{\rm min}(\kappa,\rho) = \left(1-\kappa^2\right)^2\frac{3\pi^2}{g^2\rho}, \qquad N_{\rm CS}(\kappa) = \frac{1}{4}{\rm sign}(\kappa)(1-|\kappa|)^2(2+|\kappa|), \tag{25}$$

where $\kappa = 0$ corresponds to the top of the barrier, known as the "sphaleron".

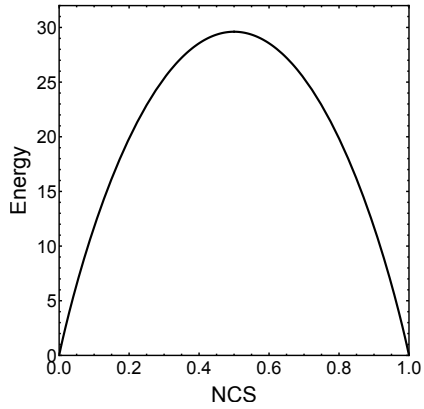

Fig. 3. The potential energy $U_{\rm min}(N_{\rm CS},\rho)$ (in units of $1/g^2\rho$) *versus* the Chern–Simons number $N_{\rm CS}$ for the "sphaleron path" between $N_{\rm CS}=0$ and $N_{\rm CS}=1$.

Production of sphaleron-path states can be described semi-classically using instanton–anti-instanton "streamline" [17, 25, 26] and their explosion in Minkowski space-time by [27]. The new results consist in estimates of how one can produce QCD sphalerons, as topologically-charged clusters in double-diffractive events, with a cluster of few GeV mass at the center. Its decay modes into multiple 3-mesons channels were calculated using the 't Hooft Lagrangian [24].

4. Mesons and baryon light-front wave functions and isospin asymmetry of the nucleon "sea"

High-energy processes, as in the famed electron–nucleon deep inelastic scattering, produced a rich "parton phenomenology" in the form of parton distribution functions (PDFs), distribution amplitudes (DAs), trans-

verse momentum distribution (TMDs), *etc.* They are pertinent matrix elements of light-front wave functions (LFWFs), which are not well understood from first principles. In [28, 29], light-front DAs and PDFs were explored in the instanton liquid model using the large momentum effective theory (LaMET) formulation [30], although the LaMET matching kernels may well be contaminated by nonperturbative small size instanton and anti-instanton contributions (also $\bar{I}I$ molecules as we discuss below) [31].

Furthermore, the understanding of the light-front Hamiltonians is only in its initial stage. In [32], LFWFs for several mesons and baryons were calculated, including for the first time the 5-quark component of the baryon, in relation to the *isospin asymmetry puzzle*. The canonical process of quark pair production via gluons is "flavor blind", and yet the anti-quark sea of the nucleon is very asymmetric, as shown in Fig. 4 (right). As noted in [33], the 't Hooft Lagrangian is *flavor asymmetric*, say a d quark can produce a $\bar{u}u$ pair (Fig. 4 (left)) but *not* a $\bar{d}d$. If it would be the only process, the $\bar{d}/\bar{u}$ ratio would be 2, as there are two u quarks and only one d in the nucleon. This observation is not very far from the currently reported data for $x \sim 0.2$.

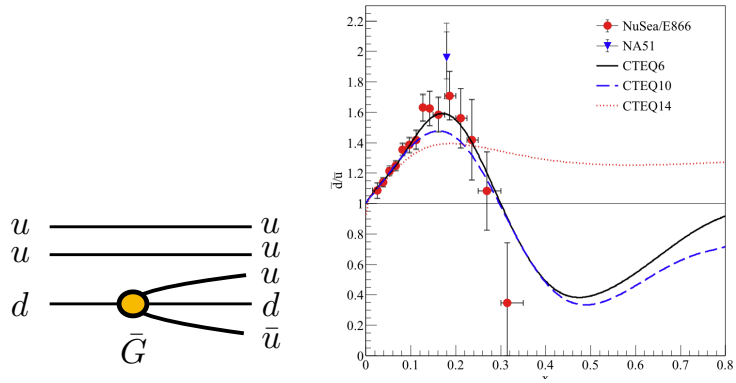

Fig. 4. Sea generation via the 't Hooft Lagrangian (left) and the data on the $\bar{d}/\bar{u}$ ratio *versus* the antiquark momentum fraction x (right).

A calculation [32] of the admixture of the 5-q states to the nucleon LFWF leads to the right magnitude for the asymmetry and shape of the first-generation anti-quarks in agreement with the data.

5. "Dense instanton ensemble"

The original instanton liquid model focused on the quark condensate and chiral symmetry breaking and, therefore, on the stand-alone instantons, whose zero modes get collectivized. But the instanton ensemble also includes close instanton–anti-instanton pairs or molecules. In so far, the application

of the "molecular component" of the semiclassical ensemble was made only in connection to the phase transitions in hot/dense matter. Indeed, this component is the only one which survives at temperatures $T > T_c$, where chiral symmetry is restored. Account for both components together started with [35]. The "molecular component" was also shown to be important at high baryonic densities, where it contributes to quark pairing and color superconductivity [36].

The $\bar{I}I$ molecules were also observed on the lattice. The stand-alone instantons are seen via "deep cooling", during which the instanton–anti-instanton molecules get annihilated. The close $\bar{I}I$ pairs have been qualitatively studied in the recent work [37], which studied their evolution during cooling, see Fig. 5. When extrapolated to zero cooling (left-hand side of the plots), one sees that while the instanton size fits previous expectations (23), the density seems to actually be significantly larger.

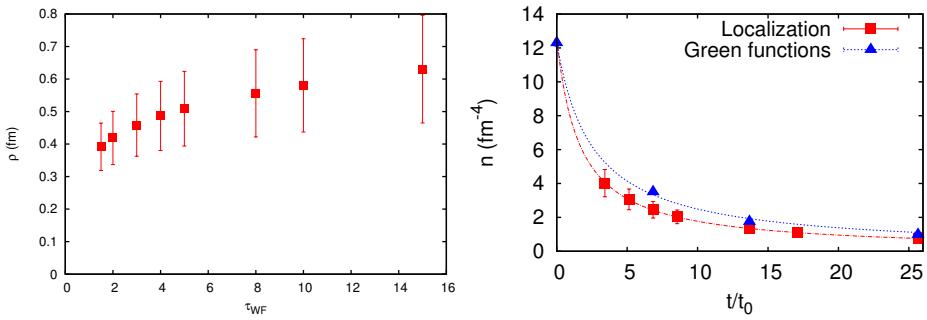

Fig. 5. The dependence of the mean instanton sizes (left) and density (right) on the gradient flow cooling time $\tau = t/t_0$ (arbitrary units). The quantum vacuum corresponds to an extrapolation to $\tau \to 0$.

6. Form factors: including instantons in the hard block

More recently, we have explored the nonperturbative contributions to the "hard block" of mesonic form factors [38]. We calculated the photon, scalar, graviton and dilaton FFs for the pion, rho, and scalar a_0 (brother of η'). The field at the instanton center is rather strong

$$G_{\rm rms} \equiv \sqrt{\left(G^a_{\mu\nu}(0)\right)^2} = \sqrt{192}/\rho^2 \approx 5 \text{ GeV}^2 \,,$$

for a typical size of $\rho = 1/3$ fm. This scale is comparable to Q^2 in the so-called semi-hard region.

One example, which was studied a lot experimentally, is the electromagnetic pion form factor, shown in Fig. 6 (right). It is dominated by the diagram with three propagators made of nonzero Dirac modes (the left-most), not the one with Dirac zero modes (in the middle). The contributions of the "dense instanton liquid", through $\kappa = \pi^2 n_{I+\bar{I}} \rho^4 \to 1$, are shown by the middle curve in Fig. 6 (right). The sum of the perturbative and instanton-induced form factor reproduces the data.

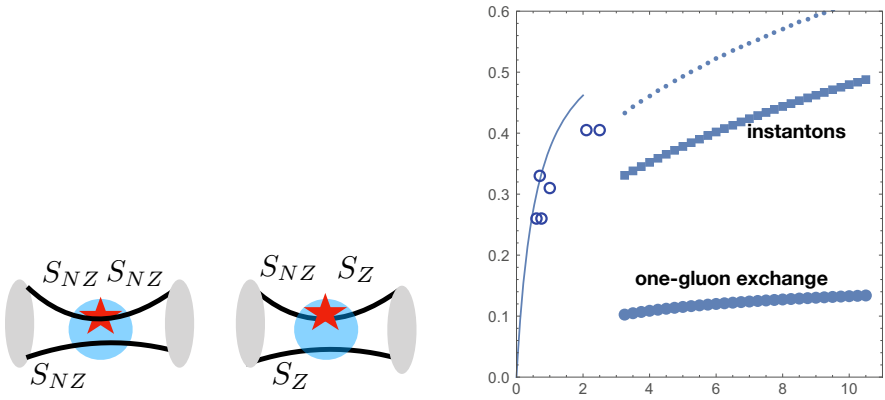

Fig. 6. Left: Two diagrams with quark propagators in the instanton fields. Right: Vector form factor of the pion $Q^2 F_\pi(Q^2)$. Open points correspond to some experimental data points, thin curve on the left is a standard dipole fit. The dotted line at the top is the sum of the perturbative and instanton contributions

The expressions for the perturbative, nonzero-mode and zero-mode parts are

$$
\begin{aligned}
V_a^\pi\left(Q^2\right) \;=\; & \epsilon_\mu(q)\left(p^\mu + p'^\mu\right)\left(e_u + e_{\bar{d}}\right)\left[\left(\frac{2C_{\rm F}\pi\alpha_{\rm s}f_\pi^2}{N_{\rm c}Q^2}\right)\right. \\
& \times \int {\rm d}x_1 {\rm d}x_2 \left(\frac{1}{\bar{x}_1\bar{x}_2 + m_{\rm gluon}^2/Q^2}\right)\left(\varphi_\pi(x_1)\varphi_\pi(x_2)\right. \\
& +2\frac{\chi_\pi^2}{Q^2}\left(\varphi_\pi^{\rm P}(x_1)\varphi_\pi^{\rm P}(x_2)\left(\frac{1}{\bar{x}_2 + E_\perp^2/Q^2} - 1\right)\right. \\
& \left.\left.\left.+\frac{1}{6}\varphi_\pi^{\rm P}(x_1)\varphi_\pi'^{\rm T}(x_2)\left(\frac{1}{\bar{x}_2 + E_\perp^2/Q^2} + 1\right)\right)\right)\right],
\end{aligned}
\tag{26}
$$

$$V_c^\pi = \epsilon_\mu(q)\left(p^\mu + p'^\mu\right)(e_u + e_{\bar{d}})\left[\frac{\kappa\pi^2 f_\pi^2 \chi_\pi^2}{N_c M_Q^2}\left\langle \rho^2 \mathbb{G}_V(Q\rho)\right\rangle \right.$$
$$\left. \times \int \mathrm{d}x_1 \mathrm{d}x_2 \bar{x}_1 \left(\varphi_\pi^{\mathrm{P}}(x_1)\varphi_\pi^{\mathrm{P}}(x_2) - \frac{1}{36}\varphi_\pi^{'\mathrm{T}}(x_1)\varphi_\pi^{'\mathrm{T}}(x_2)\right)\right], \tag{27}$$

$$V_d^\pi = -\epsilon_\mu(q)\left(p^\mu + p'^\mu\right)(e_u + e_{\bar{d}})$$
$$\times \left[\left(\frac{1}{N_c^2(N_c+1)}\right)\frac{4\kappa\pi^2 f_\pi^2 \chi_\pi^2}{3M_Q^2}\left\langle \rho^2 \frac{K_1(Q\rho)}{Q\rho}\right\rangle \int \mathrm{d}x_1 \mathrm{d}x_2 \varphi_\pi^{\mathrm{P}}(x_1)\varphi_\pi^{'T}(x_2)\right]. \tag{28}$$

Here, $\varphi_\pi^{\mathrm{P}}, \varphi_\pi^T$ are the pion DAs associated with the pseudoscalar γ_5 and tensor $\sigma^{\mu\nu}$ channels. The leading twist φ_π is the standard matrix element of the axial current $\gamma_\mu\gamma_5$. In Fig. 6, all three DAs are taken to be just constant, independent of x. (Therefore, all tensor DAs with an x-derivative vanish.)

7. Instanton-induced inter-quark forces

Historically, hadronic spectroscopy got a solid foundation in 1970s with the discovery of nonrelativistic quarkonia made of heavy c, b quarks. In the first approximation, those are well described by the simple Cornell potential

$$V_{\mathrm{Cornell}}(r) = -\frac{4\alpha_{\mathrm{s}}}{3}\frac{1}{r} + \sigma_{\mathrm{T}} r\,, \tag{29}$$

which correctly attributes the short-distance potential to the perturbative gluon exchange, and its large-distance $\mathcal{O}(r)$ contribution to the tension of a confining flux tube (the QCD string). The issues to be discussed deal with the nonperturbative origins of the inter-quark interactions at *intermediate* distances $r \sim 0.2$–0.5 fm.

Later developments in [39, 40] connected the static inter-quark potential to the correlator of static Wilson lines (central)

$$\mathrm{e}^{-V_{\mathrm{C}}(r)T} = \left\langle W\left(\vec{x}_1\right) W^\dagger\left(\vec{x}_2\right)\right\rangle . \tag{30}$$

The spin-dependent forces were related to such correlators with two magnetic fields ($V_{\mathrm{SS}}, V_{\mathrm{tensor}}$), or a magnetic and electric field for the spin–orbit one. To evaluate such nonlocal quantities, one needs to use lattice simulations or rely on a certain model of the vacuum fields. In Fig. 7 (left), we show the predictions from a "dense instanton model" to the central potential compared to the linear potential, and its version from [41] including the string quantum vibrations (resummed "Lusher terms"). One can see that instantons can complement smoothly the flux tube at intermediate distances.

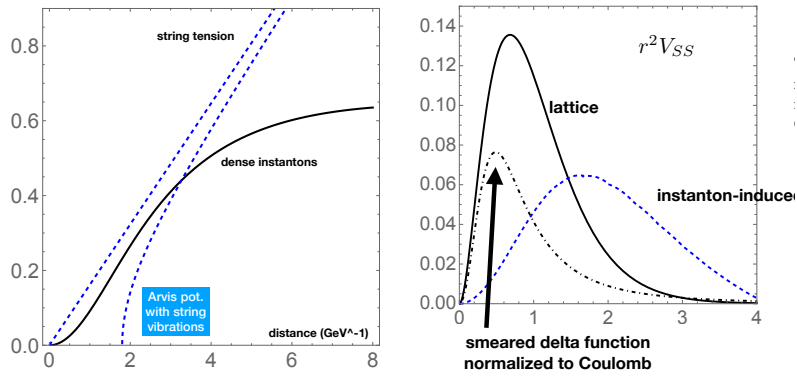

Flavors	$M_\Upsilon - M_{\eta_b}$	$M_{J/\psi} - M_{\eta_c}$	$M(D^*) - M(D)$	$M(K^*) - M(K)$	$M(\rho) - M(\pi)$
Exp.	61.	116.	137.	398.	636.
$\langle V_{\rm SS}^{\rm lat} \rangle / 3M_1M_2$	46.	108.	98.	170.	
$\left\langle \vec{\nabla}^2 V_{\rm C} \right\rangle / 3M_1M_2$	28.	58.	48.	82.	
$\left\langle \vec{\nabla}^2 V_{\rm inst} \right\rangle / 3M_1M_2$	7.	30.	48.	90.	

Fig. 7. The central potential $V_{\rm C}$ (left) and spin–spin $r^2V_{\rm SS}(r)$ (right) *versus* distance r, (GeV^{-1}). The lattice result is one of the parameterization, given in [42], the perturbative is the Laplacian of (regulated) Coulomb term.

One problem with the electric flux tube model is that it does not provide magnetic fields, while instantons are self-dual and have B (as large as E) badly needed to generate the spin forces. We calculated the instanton contributions to spin forces, see $V_{\rm SS}$, in comparison to the lattice potential, perturbative and instanton-induced in Fig. 7 (right). Note that the area below the perturbative and instanton-induced terms is comparable. The corresponding matrix elements (using the Cornell wave functions with proper quark masses) are shown in the table. One can see that *e.g.* for charmonium, the magntitude of the spin–spin term is in agreement with the lattice estimate and the level splitting. We also considered the $L = 1$ families of mesons, from heavy to light, and considered other spin-dependent potentials. We also discussed $\bar{I}I$ molecules, which provide somewhat different potentials due to their different field content.

However, for heavy–light and light–light cases, this $V_{\rm SS}$ is not enough. The missing part is attributed to the part of the quark propagators containing zero modes (the 't Hooft Lagrangian). It works well for heavy–light and the pions, as expected.

8. Hadrons on the light front

In the rest frame, the nonrelativistic description of hadrons and their constituents is most natural for heavy quarks, with the use of nonrelativistic kinetic energy and potentials. However, this approach is not justified for light quarks, as masses and transverse momenta are comparable. Their quantum motion is complicated as illustrated in Fig. 8 (left). The situation however is much more "democratic" on the light front, where all constituents motion are frozen anyway in Fig. 8 (right). All interactions can be deduced from the pertinent Wilson loops and modulo tunneling due to zero modes.

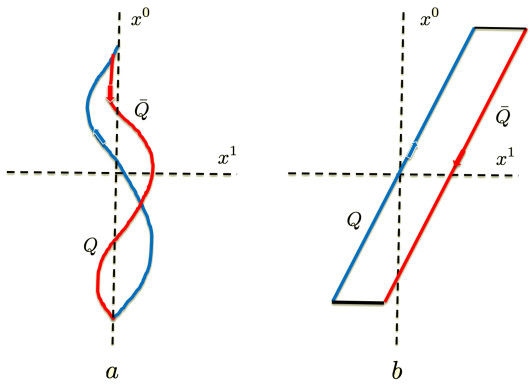

Fig. 8. $\bar{Q}Q$ meson in the rest frame (left) and in the light-front frame (right).

8.1. Light-front Hamiltonian from the QCD vacuum

Indeed, let $Q\bar{Q} \equiv Q_1 Q_2$ be the world lines assigned to the Wilson lines composing a meson in Fig. 8 (right). In the Euclidean signature, the Wilson lines are sloped at an angle θ, and their light-like limit follows by analytical continuation from Euclidean angle to Minkowskian rapidity $\theta \to -i\chi$ [34, 43–45]. For the squared meson mass operator or light-front Hamiltonian $H_{\rm LF}$, the result is [34]

$$H_{\rm LF} \approx \frac{k_\perp^2 + m_Q^2}{x\bar{x}} + 2P^+P^- \approx \frac{k_\perp^2 + m_Q^2}{x\bar{x}} + 2M(\mathbb{V}_{Cg}(\xi_x) + \mathbb{V}_{\rm C}(\xi_x) + \mathbb{V}_{\rm SD}(\xi_x, b_\perp) + \mathbb{V}_{\rm TH}(\xi_x, b_\perp)) \,. \quad (31)$$

On the light front, the invariant distance ξ_x is

$$M\xi_x = \left(|i\mathrm{d}/\mathrm{d}x|^2 + M^2 {b_\perp}^2 \right)^{\frac{1}{2}} \,. \quad (32)$$

The longitudinal distance $\gamma b_3 = i\mathrm{d}/\mathrm{d}x/M$ is the conjugate of Björken-x or $x = k^3/P^3$.

The one-gluon exchange potential V_{Cg} in the instanton vacuum is

$$\mathbb{V}_{Cg}(\xi_x)=-\frac{g^2T_1^AT_2^A}{2\pi^2}\frac{1}{\xi_x}\int\limits_0^\infty\frac{\mathrm{d}x\,x\mathrm{sin}x}{x^2+(\xi_x m_G(x\rho/\xi_x))^2}\to-\frac{g^2T_1^AT_2^A}{4\pi}\frac{\mathrm{e}^{-m_G\xi_x}}{\xi_x}\,, \tag{33}$$

with the running gluon mass [46]

$$\begin{aligned} m_G(k\rho) &= m_G\left(k\rho\,K_1(k\rho)\right)\,,\\ m_G\rho &\approx 2\left(\frac{6\kappa}{N_c^2-1}\right)^{\frac{1}{2}}\approx 0.55 \end{aligned} \tag{34}$$

using the estimate $\kappa=\pi^2\rho^4 n_{I+\bar I}$ in the right-most result.

The instanton-induced central potential $V_{\rm C}$ is

$$\mathbb{V}_{\rm C}(\xi_x)=\left(\frac{4\kappa}{N_c\rho}\right)\boldsymbol{H}\left(\tilde\xi_x\right)\,, \tag{35}$$

with the integral operator

$$\begin{aligned} \boldsymbol{H}(\xi_x)=&\int\limits_0^\infty y^2\mathrm{d}y\int\limits_{-1}^{+1}\mathrm{d}t\\ &\times\left[1-\cos\left(\frac{\pi y}{\sqrt{y^2+1}}\right)\cos\left(\pi\left(\frac{y^2+\tilde\xi_x^2+2\xi_x yt}{y^2+\tilde\xi_x^2+2\tilde\xi_x yt+1}\right)^{\frac{1}{2}}\right)\right.\\ &\left.-\frac{y+\xi_x t}{\left(y^2+\xi_x^2+2\tilde\xi_x yt\right)^{\frac{1}{2}}}\sin\left(\frac{\pi y}{\sqrt{y^2+1}}\right)\sin\left(\pi\left(\frac{y^2+\tilde\xi_x^2+2\tilde\xi_x yt}{y^2+\xi_x^2+2\tilde\xi_x yt+1}\right)^{\frac{1}{2}}\right)\right], \end{aligned} \tag{36}$$

with the dimensionless invariant distance on the light front $\tilde\xi_x=\xi_x/\rho$. $\boldsymbol{H}(\tilde\xi_x)$ admits the short-distance limit

$$\boldsymbol{H}(\tilde\xi_x)\approx+\left(\frac{\pi^3}{48}-\frac{\pi^3}{3}J_1(2\pi)\right)\tilde\xi_x^2+\left(-\frac{\pi^3\left(438+7\pi^2\right)}{30720}+\frac{J_2(2\pi)}{80}\right)\tilde\xi_x^4 \tag{37}$$

and the large-distance limit

$$\boldsymbol{H}(\xi_x)\approx-\frac{2\pi^2}{3}\left(\pi J_0(\pi)+J_1(\pi)\right)+\frac{C}{\tilde\xi_x^p} \tag{38}$$

with $p \ll 1$ and $C > 0$. The large asymptotic is to be subtracted in the definition of the potential. In the dense instanton vacuum [34], the central potential (35) is almost linear at intermediate distances of 0.2–0.5 fm, and is expected to be taken over by the linearity of the confining potential at larger distances.

The spin potentials receive a contribution from both the perturbative and nonperturbative parts of the underlying gluonic fields. In particular, the nonperturbative instanton-induced spin potentials can be derived in a closed form

$$\mathbb{V}_{\rm SD}(\xi_x, b_\perp) = 2M\Bigg(\left(\frac{l_{1\perp}\cdot S_{2\perp}}{m_{Q1}m_{Q2}} - \frac{l_{2\perp}\cdot S_{1\perp}}{m_{Q1}m_{Q2}} \right) \frac{1}{\xi_x} \mathbb{V}'_{\rm C}(\xi_x) + \frac{1}{m_{Q1}m_{Q2}} \left(\left(S_{1\perp}\cdot \hat{b}_\perp \right) \left(S_{2\perp}\hat{b}_\perp \right) - \frac{1}{2} S_{1\perp}\cdot S_{2\perp} \right) \frac{2b_\perp^2}{\xi_x} \mathbb{V}''_{\rm C}(\xi_x) \Bigg) \tag{39}$$

with the respective spins $\vec{S}_{1,2} = \vec{\sigma}_{1,2}/2$ and transverse orbital momenta

$$l_{1,2\perp} = \pm \left(b_\perp \times m_{Q1,2} s_{1,2} \hat{3} \right)_\perp , \qquad s_{1,2} = {\rm sgn}(v_{1,2}) \to \frac{M x_{1,2}}{m_{Q1,2}} . \tag{40}$$

The contributions stemming from the zero modes $\mathbb{V}_{\rm TH}(\xi_x, b_\perp)$ are not included. They follow from the 't Hooft determinantal interaction properly continued to the light front.

8.2. Light-front spectra and wave functions

We have used the light-front Hamiltonian (31) to analyze heavy and light mesons and baryons. One strategy consists in linearizing the confining part of the potential (instanton induced at small distances and string induced at large distances), and treating the Coulomb and spin contributions perturbatively. More specifically, the central part of the potential can be redefined using the "einbein trick"

$$2M\mathbb{V}_{\rm C}(x, b_\perp) = 2\sigma_{\rm T} \left(|i{\rm d}/{\rm d}x|^2 + M^2 b_\perp^2 \right)^{\frac{1}{2}} \to \sigma_{\rm T} \left(\frac{|i{\rm d}/{\rm d}x|^2 + b\, b_\perp^2}{a} + a \right) \tag{41}$$

with a, b variational parameters. The minimization with respect to a would lead back to a previous expression, but the trick is to do it *after* the Hamiltonian is diagonalized. It is also followed by the substitution $b \to M^2 \approx (2m_Q)^2$ for heavy mesons and most light ones. The light-front Hamiltonian is then

$$H_{\rm LF} = H_0 + \tilde{V} + V_{\rm perp} + V_{\rm spin} , \tag{42}$$

with

$$H_0 = \frac{\sigma_{\rm T}}{a}\left(-\frac{\partial^2}{\partial x^2} - b\frac{\partial^2}{\partial \vec{k}_\perp^2}\right) + \sigma_{\rm T} a + 4\left(m_Q^2 + k_\perp^2\right) \tag{43}$$

and $\tilde{V}$

$$\tilde{V}\left(x, \vec{k}_\perp\right) \equiv \left(m_Q^2 + k_\perp^2\right)\left(\frac{1}{x\bar{x}} - 4\right), \tag{44}$$

where $\bar{x} = 1 - x$. H_0 is diagonal in the functional basis used [34]. We use the momentum representation, with $\vec{k}_\perp$ as a variable. The residual interaction has nonzero matrix elements $\langle n_1|V(x, \vec{k}_\perp)|n_2\rangle$ for all n_1, n_2 pairs. The perturbative part $V_{\rm perp}$ for heavy quarks is the Coulomb term, with running coupling and other radiative corrections. Finally, the last term $V_{\rm spin}$ contains matrices in spin variables and in orbital momenta.

To solve the problem, we have two numerical strategies. First, we used a (truncated) basis set and write the Hamiltonian in the form of a 12×12 matrix, and diagonalize $H_0 + \tilde{V}$, to find its eigenvalues as a function of the remaining parameter a. The results for the three lowest states $n = 1, 2, 3$ are shown in Fig. 9 (left). The near flatness in a around the minima suggests $a = 25$ as a common value. This procedure preserves the orthonormality of the eigen-spectrum.

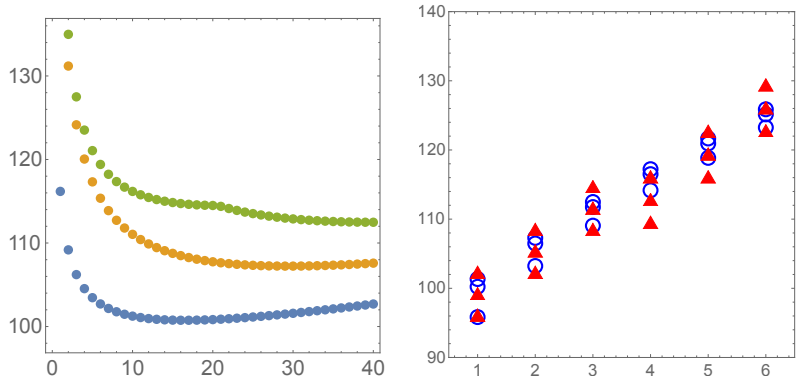

Fig. 9. Left: Squared masses M_n^2 for $\bar{b}b$ mesons for $n = 1, 2, 3$ *versus* the variational parameter a. Right: Squared masses for $n = 0 \ldots 5$ (left to right) and orbital momentum $m = 0, 1, 2$ (down to up), calculated from the light-front Hamiltonian $H_{\rm LF}$ (red triangles), and shifted by a constant, $M_{n+1}^2 - 5$ GeV^2. For comparison, the blue circles show the squared masses M_{n+1}^2 calculated from the Schrödinger equation in the CM frame, with only linear plus centrifugal potentials.

Another approach worked out later is a direct numerical solution in 3D space of transverse momenta and x. To our delight, the wave functions found in both methods agree within the width of the lines.

The calculated masses (shifted by a constant "mass renormalization", to make $n = 0$, $m = 0$ states the same) are shown in Fig. 9 (right). The right-hand side part shows good agreement between the masses obtained solving the Schrödinger equation in the rest frame (blue circles) and the masses following from the light-front frame (red triangles). The slope is correct and is determined by the same string tension $\sigma_{\rm T}$. The splittings in orbital momentum are of the same scale, but not identical. This is expected, as we compare the 2-dimensional m-states on the light front, with the 3-dimensional L-states in the center-of-mass frame. The irregularity between the third and fourth set of states is due to our use of a modest basis set, with only three radial functions (altogether 12 functions if one counts them with 4 longitudinal harmonics). This can be eliminated using a larger set. The corresponding wave function for bottomium is shown in Fig. 10 (left), and for a typical light meson $\bar{q}q$ is shown Fig. 10 (right). Further details can be found in our subsequent papers.

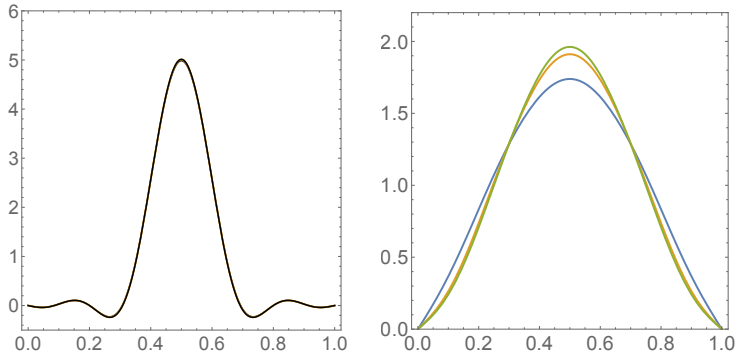

Fig. 10. Distribution amplitudes for $\bar{b}b$ (left) and a "generic" light $\bar{q}q$ meson (right) as a function of x, for the three lowest states $n = 0, 1, 2$. For the bottomium, the difference between the three curves is too small to be visible. For the light meson, the differences are visible. With increasing n, the DAs become narrower and higher at $x = \frac{1}{2}$.

9. Semiclassical theory of deconfinement and chiral phase transitions based on instanton-dyons

Instanton-dyons are topological solutions of the YM equations at finite temperatures. Their semiclassical ensembles were studied by a number of methods, including direct Monte-Carlo simulation, for SU(2) and SU(3) theories, with and without fermions. We present these results and compare them with those from lattice studies. We also consider two types of QCD deformations. One consists in adding operators with powers of the Polyakov

line, affecting deconfinement. Another consists in changing the quark periodicity condition, affecting the chiral transition. We will also discuss how lattice configurations (with realistic quark masses) can be used to unravel the zero and near-zero Dirac modes of the underlying gauge configurations. The results are in good agreement with the analytic instanton-dyon theory. In sum, the QCD phase transitions are well described in terms of such semiclassical configurations.

Remarkably, the partition function for monopoles follows from that of instanton-dyons by the *Poisson duality*, which is tightly related to the Hamilton and Jacobi duality when describing dynamical systems. More details regarding this and further discussions on the QCD flux tubes are in [1].

9.1. Instanton-dyons on the lattice

A thorough discussion of the Kraan–van Baal solution for an instanton, containing N_c instanton-dyons, or the formalism leading to their zero modes, is not possible in this short review, and we refer to the original papers for that. For completeness, we recall that the eigenvalues of Polyakov line, designated as $\mu_i(T), i = 1 \dots N_c$ can be regarded as locations on a unit circle. Their differences $\nu_i = \mu_{I+1} - \mu_i$ are lengths of the corresponding fractions of the circle, $S_i = \nu_i S$, where

$$S = \frac{8\pi^2}{g^2} = \left(\frac{11}{3}N_c - \frac{2}{3}N_f\right) \log\left(\frac{T}{\Lambda_{QCD}}\right) .$$

Also, if quarks are given different periodicity phases z_f, $f = 1 \dots N_f$ over the Matsubara circle, the normalizable physical zero mode belongs to the dyon for which z_f belongs to the sector $z_f \in [\mu_i, \mu_{i+1}]$. So, using different z_f, one can see all dyon types.

Let us start with the description of the efforts to identify these objects on the lattice. The key method is "cooling" of vacuum configurations, which was used efficiently to identify ensembles of instantons in the 1990s. The first lattice observation of instanton-dyons was via "constrained minimization" by Langfeld and Ilgenfritz [47], fixing $\langle P \rangle$, in which self-dual clusters with non-integer topological charges were seen. Gattringer *et al.* and Ilgenfritz *et al.* have since introduced and refined the "fermionic filter" allowing to identify the instanton-dyons via distinct zero modes and variable periodicity phases.

Some of the recent progress in these directions can be found in [48, 49]. QCD simulations with realistic masses were performed at and near T_c, using domain wall fermions with good chiral symmetry. Using overlap fermions with exact chiral symmetry, the focus was on exact zero modes (and near-zero ones). The left part in Fig. 11 shows a typical landscape of the zero-mode densities. There are three different dyon types for $N_c = 3$. The shape

of isolated peaks is well described by analytic formulae from van Baal and collaborators, and derived for a single dyon. They are apparently undisturbed by millions of perturbative gluons present in the ensemble.

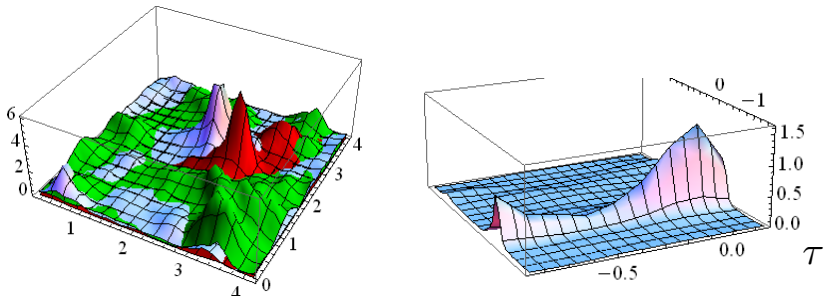

Fig. 11. Left: Space slice of density of an exact zero mode from QCD simulation at $T = T_c$. The three colors refer to dyons of three different types. Right: Tau-dependence of a dyon, perturbed by nearby dyons. See the text.

Previous works, however, have not analyzed the "topological clusters", the situations in which two or three dyons overlap strongly. The Kraan–van Baal solution presents analytic formulae for these cases, and good agreement was also found in the numerical analysis of instanton-dyon ensembles in [48, 49]. The right part in Fig. 11 is an example of a (Euclidean time) τ-dependence of the density. An isolated dyon should show no such dependence at all, and what is seen is a result of an interference with overlapping dyons. Locating those and using analytic expressions for the zero-mode density confirms their identity. The *semiclassical description of zero and near-zero Dirac modes on the lattice is quite accurate, at least in terms of the zero-mode shapes.*

9.2. Studies of instanton-dyon ensembles

The simplest limiting case is weak coupling or very high temperature ($T \to \infty$), in which the dyon density is exponentially small, with their interactions and back reactions negligible. In QCD with N_f quarks, all twist factors are equal to $z_f = \pi$ and all the L dyons combine in a 't Hooft vertex with $2N_f$ legs. For $N_f = 1$, $U(1)_A$ chiral symmetry is explicitly broken at any T, with exponentially small $\langle\bar{q}q\rangle$. For $N_f > 1$ and $SU(N_f)_A$, chiral symmetry is unbroken. Thus, there should be "molecules" $\bar{L}L$, similar to $\bar{I}I$ molecules originally discussed in [35, 50, 51], and called "bions" by Ünsal and collaborators.

The opposite case is a dense ensemble at $T \sim T_c$ discussed by mean-field approximation in a number of settings [52–54]. Here, we will only discuss the numerical simulations for the SU(2) in [55, 56] and SU(3) in [57, 58] color groups, without ($N_f = 0$) and with two quark flavors ($N_f = 2$).

The first physics issue is the *deconfinement* phase transition. Recall that the Gross–Pisarski–Yaffe (GPY) perturbative potential for the Polyakov line favors a trivial $\langle P \rangle = 1$ case and disfavors confinement l $\langle P \rangle = 0$. Therefore, to have confinement, the nonperturbative effects — with a sufficient density of the dyons in the simulations — should *overcome* the GPY potential. In Fig. 12, we see that this happens differently for SU(2) and SU(3) pure gauge theories. In the former, the minimum gradually shifts to the confining value

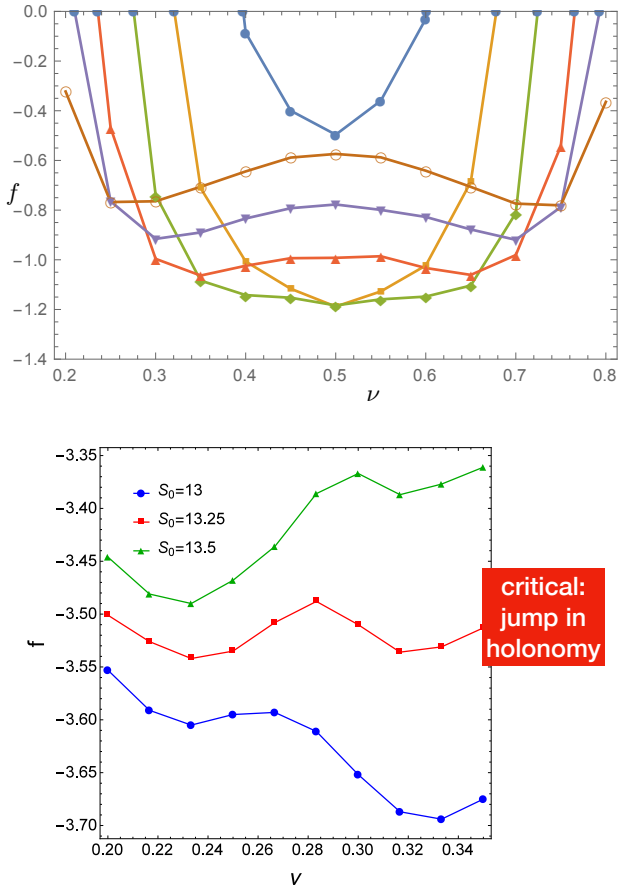

Fig. 12. Free energy f *versus* the holonomy parameter ν for SU(2) (top) and SU(3) (bottom) pure gauge theories. Different curves are for different instanton densities (or temperatures). See the text.

of $\nu = 1/2$ and stays there at high densities. In the latter, there is a jump, indicating a first-order transition. There is no place here for comparison with lattice data. We just mention that the SU(3) case $\langle P \rangle$ jumps to a value 0.4, remarkably close to the reported lattice value. The *deformation* of the SU(3) gauge theory by an operator $\sim P^2$ in the instanton-dyon ensembles is also in agreement with the lattice simulation. In particular, the deconfinement temperature is observed to increase with the size of the jump decreasing.

The second nonperturbative issue is chiral symmetry breaking at low T. Again, it requires a sufficient density of the dyons, so that their zero modes can get *collectivized*[9].

9.3. QCD deformation by modified quark periodicity phases

This deformation came first under the name of "imaginary chemical potentials" [59]. Its usage is different for *small* and *large* deformations. In the former case, the motivation was due to the fact that imaginary chemical potentials can be simulated by usual Monte-Carlo algorithms, while those with real μ cannot. A plot of the lattice results for negative $\mu^2 < 0$ allows the extrapolation to real μ, *e.g.* by Taylor series. This strategy has been used in many lattice studies.

For a large phase, Roberge and Weiss predicted a first order transitions close to $z = (2k+1)\pi/N_{\rm c}$, due to different $N_{\rm c}$ branches of the gluonic GPY potential. Of course, it is a perturbative argument expected to be true at large T only. Indeed, when dyons are numerous this transition ends, and according to [60] it happens at $T_{\rm RW} = 1.34(7)\ T_{\rm c} = 208(5)$ MeV.

Another form of deformed QCD is to select imaginary chemical potentials proportional to T, so that the quark fugacities are $\exp(iz_{\rm f})$, $f = 1 \dots N_{\rm f}$, with certain T-independent *periodic phases*. Moving from conventional $z_{\rm f} = \pi$ (quarks are fermions) to other values, one should see multiple phase transitions, each time when one of the $z_{\rm f}$ crosses the Polyakov phases $\mu_i(T)$, as the fermion zero modes jump from one instanton-dyon to another. The 'ultimate" selection for $N_{\rm c} = N_{\rm f}$ theories was proposed in [61], with $z_{\rm f}$ suggested to be located "democratically", with one phase located inside each of the holonomy sectors $[\mu_{i+1}, \mu_i]$ (for $T < T_{\rm deconfinement}$).

In Fig. 13, we show ensembles of instanton-dyons simulations for $N_{\rm c} = N_{\rm f} = 2$ QCD and Z_2QC$_2$D, with one quark being a fermion and one being a boson. The plots show drastic changes in both phase transitions. Deconfinement changes from a crossover to a strong first order, and chiral restoration

[9] Note that already in 1961, the NJL model has shown that one needs a large enough 4-fermion coupling to break chiral symmetry.

is not seen at all[10]. We note that the multiply deformed worlds (such as Z_{N_c}QCD) are unphysical and qualitatively different from ours. We expect them to be separated by singularities. Indeed, we recall that Z_{N_c}QCD has a completely different flavor and chiral symmetries (except at high T when all μ_i are near zero). Its chiral symmetry is split diagonally for all flavors $(\mathrm{U}(1)_\mathrm{A})^{N_\mathrm{f}-1}$, each broken *explicitly* by diquark 't Hooft operators for each dyon type. Obviously, this chiral symmetry breaking has no relation to the *spontaneously broken* $SU(N_f)$ *chiral symmetry* concurring in our world, and due to the multi-quark operators with finite instanton-dyon density.

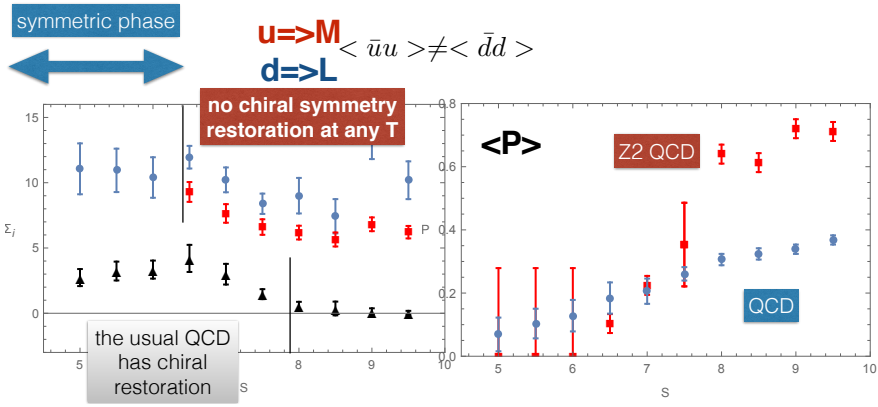

Fig. 13. Quark condensates (left) and Polyakov line (right) *versus* the action parameter $S(T)$. The higher temperatures are recorded on the right vertical axis. The blue circles in the right plot are for QCD with $N_\mathrm{c} = N_\mathrm{f} = 2$ and the red squares are for $Z_2\mathrm{QC}_2\mathrm{D}$. A *crossover* in the former, changes to a first-order transition in the latter. The black triangles on the left are for QCD with $N_\mathrm{c} = N_\mathrm{f} = 2$, with restored chiral $\mathrm{SU}(2)_\mathrm{A}$ symmetry above $S > 8$. The blue discs and red squares show two chiral condensates for $Z_2\mathrm{QC}_2\mathrm{D}$. We clearly see a transition from a symmetric to an asymmetric phase, with no chiral symmetry restoration.

Another take on these unusual phases with modified quark periodicities historically came from supersymmetry. Davies, Hollowood, and Khose [62] considered $\mathcal{N} = 1$ SYM theory on $R^3 \times S^1$ with a small circle and *bosonic* gluinos, and evaluated the quark condensate using instanton-dyons. In this case, the gluino term in the GPY potential changes sign, canceling the gluon contribution.

[10] Note that SU(2) is somewhat of a special case. If the group is SU(3) and two sectors of M_1, M_2 dyons would have z_1, z_2 located in them, ultimately at high T, these sectors shrink as $\mu_i(T)$ move towards zero. When they cross phases z_1, z_2, the zero modes would return to L dyons, and thus at infinite T would become similar to undeformed QCD, with chiral symmetry restored.

Ünsal [63] considered theories with *more than one flavor* of gluinos (adjoint fermions), $N_a > 1$. The GPY potential was found to be multiplied by $(1 - N_a)$, and for $N_a > 1$ was *inverted*, favoring confinement at weak coupling (small circle or high T). It was suggested that with confinement present both at small and large $L = 1/T$, there would be *continuity* (no phase transitions) at any L. However, lattice studies [64] have found *two* deconfined phases in between those two limits, preventing in general such continuity. The considerations based on the GPY potentials at weak coupling (high temperature), do not necessarily carry to intermediate temperatures, where the phase transitions are located.

10. Summary

The physics of instantons is now nearly 50 years old, yet we are still finding new applications in the vast land of hadronic physics. Indeed, only recently, the large contributions due to the instanton–anti-instanton molecules came to focus. Recently, we used these contributions to solve two old puzzles. Specifically, the nonperturbative nature of the quark–anti-quark potentials and the large observed mesonic form factors in the semi-hard regime with $Q^2 \sim$ few GeV^2 can be explained by these fields in the QCD vacuum.

The physics of diquarks, first appearing in connection to color superconductivity, again came to the front of spectroscopy, with recent discovery of the double charmed tetraquark state T_{cc} made of $cc\bar{u}\bar{d}$.

The development of light-front Hamiltonians and wave functions entered a stage at which properties of *all* hadrons, from bottomonium to pions, and with all kinds of baryons and exotica can be systematically calculated. The traditional distinction between heavy and light physics (absence of nonrelativism in the former case) is no longer present on the light front, so all of them are studied in the same setting.

Methods for solving the corresponding equations include variational ones, diagonalization of Hamiltonian written as matrices in an appropriate basis, and even direct numerical solutions. This new "spectroscopy on the light-front" program is going to bridge the gap between the usual spectroscopy, the Euclidean version (lattice and instantons) and the light-front observables.

The semiclassical theory based on ensembles of instanton-dyons reproduces semi-quantitatively the main lattice findings of deconfinement in pure gauge theories and chiral phase transitions in QCD with light quarks. Deforming QCD by an extra action with powers of the Polyakov loop shift/modify the deconfinement transition. Deforming it via quark periodicity phases leads to phases with drastically different deconfinement and chiral transitions. While all these phases have multiple unphysical properties, their

existence shed light on the mechanisms driving the QCD phase transitions. Their key feature are "jumps" of the fermion zero modes, from one dyon type to another.

The dyon zero modes from lattice QCD simulations preserve remarkably well their shapes on the lattice, even in the case of their strong overlaps. Millions of thermal gluons do not seem to affect them.

Finally, we note that instanton-dyon simulations are simple multiple integrals over the instanton-dyon collective variables. Thus, it is relatively easy to get to say $N_d \sim 300$ of instanton-dyons. In contrast, the lattice simulations which are of course based on first principles, their current cost limits them to about $N_d \sim O(10)$ instanton-dyons, as *e.g.* seen from Fig. 2. If the instanton-dyon ensembles are important for QCD phase transitions as we suggest, then their current values for N_d are perhaps too small to get an accurate description of their phases.

There seems to be enough new land to cover for the next 50 years.

This is an extended version of the lecture presented at the 61$^{\text{st}}$ Cracow School of Theoretical Physics on the Electron–Ion Collider Physics, September 20—24, 2022, on-line.

REFERENCES

[1] E. Shuryak, «Nonperturbative Topological Phenomena in QCD and Related Theories», *Lect. Notes Phys.* **977**, 1 (2021).

[2] E.V. Shuryak, «Toward the quantitative theory of the instanton liquid IV. Tunneling in the double well potential», *Nucl. Phys. B* **302**, 621 (1988).

[3] F. Sauter, «Über das Verhalten eines Elektrons im homogenen elektrischen Feld nach der relativistischen Theorie Diracs», *Z. Phys.* **69**, 742 (1931).

[4] A.M. Polyakov, «Quark confinement and topology of gauge groups», *Nucl. Phys. B* **120**, 429 (1977).

[5] A.I. Vainshtein, V.I. Zakharov, V.A. Novikov, M.A. Shifman, «ABC of instantons», *Sov. Phys. Usp.* **25**, 195 (1982).

[6] A.A. Aleinikov, E.V. Shuryak, «Instantons in Quantum Mechanics. Two Loop E», *Yad. Fiz.* **46**, 122 (1987) (in Russian).

[7] C.F. Wöhler, E. Shuryak, «Two-loop correction to the instanton density for the double well potential», *Phys. Lett. B* **333**, 467 (1994), arXiv:hep-ph/9402287.

[8] M.A. Escobar-Ruiz, E. Shuryak, A.V. Turbiner, «Three-loop correction to the instanton density. I. The quartic double well potential», *Phys. Rev. D* **92**, 025046 (2015), *Erratum ibid.* **92**, 089902 (2015), arXiv:1501.03993 [hep-th].

[9] A.A. Belavin, A.M. Polyakov, A.S. Schwartz, Y.S. Tyupkin, «Pseudoparticle solutions of the Yang–Mills equations», *Phys. Lett. B* **59**, 85 (1975).

[10] G. 't Hooft, «Computation of the quantum effects due to a four-dimensional pseudoparticle», *Phys. Rev. D* **14**, 3432 (1976), *Erratum ibid.* **18**, 2199 (1978).

[11] E. Shuryak, J.M. Torres-Rincon, «Baryon preclustering at the freeze-out of heavy-ion collisions and light-nuclei production», *Phys. Rev. C* **101**, 034914 (2020), arXiv:1910.08119 [nucl-th].

[12] M.A. Escobar-Ruiz, E. Shuryak, A.V. Turbiner, «Quantum and thermal fluctuations in quantum mechanics and field theories from a new version of semiclassical theory», *Phys. Rev. D* **93**, 105039 (2016), arXiv:1601.03964 [hep-th].

[13] Y. Nambu, G. Jona-Lasinio, «Dynamical Model of Elementary Particles Based on an Analogy with Superconductivity. I.», *Phys. Rev.* **122**, 345 (1961).

[14] E.V. Shuryak, «The role of instantons in quantum chromodynamics. (III). Quark–gluon plasma», *Nucl. Phys. B* **203**, 140 (1982).

[15] T. Schäfer, E.V. Shuryak, «Instantons in QCD», *Rev. Mod. Phys.* **70**, 323 (1998), arXiv:hep-ph/9610451.

[16] E.V. Shuryak, «Correlation functions in the QCD vacuum», *Rev. Mod. Phys.* **65**, 1 (1993).

[17] E.V. Shuryak, J.J.M. Verbaarschot, «Baryon number violation and nonperturbative weak processes at Superconducting Super Collider energies», *Phys. Rev. Lett.* **68**, 2576 (1992).

[18] E.V. Shuryak, J.J.M. Verbaarschot, «Quark propagation in the random instanton vacuum», *Nucl. Phys. B* **410**, 37 (1993), arXiv:hep-ph/9302238.

[19] E.V. Shuryak, J.J.M. Verbaarschot, «Mesonic correlation functions in the random instanton vacuum», *Nucl. Phys. B* **410**, 55 (1993), arXiv:hep-ph/9302239.

[20] T. Schäfer, E.V. Shuryak, J.J.M. Verbaarschot, «Baryonic correlators in the random instanton vacuum», *Nucl. Phys. B* **412**, 143 (1994), arXiv:hep-ph/9306220.

[21] V. Thorsson, I. Zahed, «Diquarks in the Nambu–Jona-Lasinio model», *Phys. Rev. D* **41**, 3442 (1990).

[22] T. Schäfer, E.V. Shuryak, «Phases of QCD at high baryon density», *Lect. Notes Phys.* **578**, 203 (2001), arXiv:nucl-th/0010049.

[23] D.M. Ostrovsky, G.W. Carter, E.V. Shuryak, «Forced tunneling and turning state explosion in pure Yang–Mills theory», *Phys. Rev. D* **66**, 036004 (2002), arXiv:hep-ph/0204224.

[24] E. Shuryak, I. Zahed, «How to observe the QCD instanton/sphaleron processes at hadron colliders?», arXiv:2102.00256 [hep-ph].

[25] J.J.M. Verbaarschot, «Streamlines and conformal invariance in Yang–Mills theories», *Nucl. Phys. B* **362**, 33 (1991), *Erratum ibid.* **386**, 236 (1992).

[26] V.V. Khoze, A. Ringwald, «Valley trajectories in gauge theories», CERN-TH-6082-91.

[27] E. Shuryak, I. Zahed, «Prompt quark production by exploding sphalerons», *Phys. Rev. D* **67**, 014006 (2003), arXiv:hep-ph/0206022.

[28] A. Kock, Y. Liu, I. Zahed, «Pion and kaon parton distributions in the QCD instanton vacuum», *Phys. Rev. D* **102**, 014039 (2020), arXiv:2004.01595 [hep-ph].

[29] A. Kock, I. Zahed, «Pion and kaon distribution amplitudes up to twist-3 in the QCD instanton vacuum», *Phys. Rev. D* **104**, 116028 (2021), arXiv:2110.06989 [hep-ph].

[30] X. Ji, «Parton Physics on a Euclidean Lattice», *Phys. Rev. Lett.* **110**, 262002 (2013), arXiv:1305.1539 [hep-ph].

[31] Y. Liu, I. Zahed, «Small size instanton contributions to the quark quasi-PDF and matching kernel», arXiv:2102.07248 [hep-ph].

[32] E. Shuryak, «Light-front wave functions of mesons, baryons, and pentaquarks with topology-induced local four-quark interaction», *Phys. Rev. D* **100**, 114018 (2019), arXiv:1908.10270 [hep-ph].

[33] A.E. Dorokhov, N.I. Kochelev, «Instanton induced asymmetric quark configurations in the nucleon and parton sum rules», *Phys. Lett. B* **304**, 167 (1993).

[34] E. Shuryak, I. Zahed, «Hadronic structure on the light-front II: QCD strings, Wilson lines and potentials», arXiv:2111.01775 [hep-ph].

[35] E.M. Ilgenfritz, E.V. Shuryak, «Chiral symmetry restoration at finite temperature in the instanton liquid», *Nucl. Phys. B* **319**, 511 (1989).

[36] R. Rapp, T. Schäfer, E. Shuryak, M. Velkovsky, «Diquark Bose Condensates in High Density Matter and Instantons», *Phys. Rev. Lett.* **81**, 53 (1998), arXiv:hep-ph/9711396.

[37] A. Athenodorou *et al.*, «Instanton liquid properties from lattice QCD», *J. High Energy Phys.* **1802**, 140 (2018), arXiv:1801.10155 [hep-lat].

[38] E. Shuryak, I. Zahed, «Nonperturbative quark–antiquark interactions in mesonic form factors», *Phys. Rev. D* **103**, 054028 (2021), arXiv:2008.06169 [hep-ph].

[39] C.G. Callan, Jr. *et al.*, «The effect of instantons on the heavy quark potential», *Phys. Rev. D* **18**, 4684 (1978).

[40] E. Eichten, F. Feinberg, «Spin-dependent forces in QCD», *Phys. Rev. D* **23**, 2724 (1981).

[41] J.F. Arvis, «The exact $q\bar{q}$ potential in Nambu string theory», *Phys. Lett. B* **127**, 106 (1983).

[42] T. Kawanai, S. Sasaki, «Potential description of charmonium and charmed-strange mesons from lattice QCD», *Phys. Rev. D* **92**, 094503 (2015), arXiv:1508.02178 [hep-lat].

[43] E. Meggiolaro, «The analytic continuation of the high-energy quark–quark scattering amplitude», *Eur. Phys. J. C* **4**, 101 (1998), arXiv:hep-th/9702186.

[44] E. Shuryak, I. Zahed, «Instanton induced effects in QCD high-energy scattering», *Phys. Rev. D* **62**, 085014 (2000), arXiv:hep-ph/0005152.

[45] M. Giordano, E. Meggiolaro, «Euclidean–Minkowskian duality of Wilson-loop correlation functions», *eCONF* **C0906083**, 31 (2009), arXiv:0909.3710 [hep-ph].

[46] M. Musakhanov, U. Yakhshiev, «Gluons, light and heavy quarks in the instanton vacuum», *Int. J. Mod. Phys. E* **30**, 2141005 (2021), arXiv:2103.16628 [hep-ph].

[47] K. Langfeld, E.M. Ilgenfritz, «Confinement from semiclassical gluon fields in SU(2) gauge theory», *Nucl. Phys. B* **848**, 33 (2011), arXiv:1012.1214 [hep-lat].

[48] R.N. Larsen, S. Sharma, E. Shuryak, «The topological objects near the chiral crossover transition in QCD», *Phys. Lett. B* **794**, 14 (2019), arXiv:1811.07914 [hep-lat].

[49] R.N. Larsen, S. Sharma, E. Shuryak, «Towards a semiclassical description of QCD vacuum around T_c», *Phys. Rev. D* **102**, 034501 (2020), arXiv:1912.09141 [hep-lat].

[50] E.M. Ilgenfritz, E.V. Shuryak, «Quark induced correlations between instantons drive the chiral phase transition», *Phys. Lett. B* **325**, 263 (1994), arXiv:hep-ph/9401285.

[51] M. Velkovsky, E. Shuryak, «QCD with large number of quarks: effects of the instanton–anti-instanton pairs», *Phys. Lett. B* **437**, 398 (1998), arXiv:hep-ph/9703345h.

[52] Y. Liu, E. Shuryak, I. Zahed, «Confining dyon–antidyon Coulomb liquid model. I.», *Phys. Rev. D* **92**, 085006 (2015), arXiv:1503.03058 [hep-ph].

[53] Y. Liu, E. Shuryak, I. Zahed, «Light quarks in the screened dyon–antidyon Coulomb liquid model. II.», *Phys. Rev. D* **92**, 085007 (2015), arXiv:1503.09148 [hep-ph].

[54] Y. Liu, E. Shuryak, I. Zahed, «Dense instanton-dyon liquid model: Diagrammatics», *Phys. Rev. D* **98**, 014023 (2018), arXiv:1802.00540 [hep-ph].

[55] R. Larsen, E. Shuryak, «Interacting ensemble of the instanton-dyons and the deconfinement phase transition in the SU(2) gauge theory», *Phys. Rev. D* **92**, 094022 (2015), arXiv:1504.03341 [hep-ph].

[56] R. Larsen, E. Shuryak, «Instanton-dyon ensemble with two dynamical quarks: The chiral symmetry breaking», *Phys. Rev. D* **93**, 054029 (2016), arXiv:1511.02237 [hep-ph].

[57] D. DeMartini, E. Shuryak, «Deconfinement phase transition in the SU(3) instanton–dyon ensemble», *Phys. Rev. D* **104**, 054010 (2021), arXiv:2102.11321 [hep-ph].

[58] D. DeMartini, E. Shuryak, «Chiral symmetry breaking and confinement from an interacting ensemble of instanton dyons in two-flavor massless QCD», *Phys. Rev. D* **104**, 094031 (2021), arXiv:2108.06353 [hep-ph].

[59] A. Roberge, N. Weiss, «Gauge Theories With Imaginary Chemical Potential and the Phases of QCD», *Nucl. Phys. B* **275**, 734 (1986).

[60] C. Bonati *et al.*, «Roberge–Weiss endpoint at the physical point of $N_{\rm f} = 2+1$ QCD», *Phys. Rev. D* **93**, 074504 (2016), arXiv:1602.01426 [hep-lat].

[61] H. Kouno *et al.*, «Confinement and $\mathbb{Z}_3$ symmetry in three-flavor QCD», *J. Phys. G: Nucl. Part. Phys.* **40**, 095003 (2013), arXiv:1301.4013 [hep-ph].

[62] N.M. Davies, T.J. Hollowood, V.V. Khoze, M.P. Mattis, «Gluino condensate and magnetic monopoles in supersymmetric gluodynamics», *Nucl. Phys. B* **559**, 123 (1999), arXiv:hep-th/990501.

[63] M. Ünsal, «Magnetic bion condensation: A new mechanism of confinement and mass gap in four dimensions», *Phys. Rev. D* **80**, 065001 (2009), arXiv:0709.3269 [hep-th].

[64] G. Cossu, M. D'Elia, «Finite size phase transitions in QCD with adjoint fermions», *J. High Energy Phys.* **07**, 048 (2009), arXiv:0904.1353 [hep-lat].

[65] A. Cherman, T. Schäfer, M. Ünsal, «Chiral Lagrangian from Duality and Monopole Operators in Compactified QCD», *Phys. Rev. Lett.* **117**, 081601 (2016), arXiv:1604.06108 [hep-th].